A Soil Moisture Retrieval Method for Reducing Topographic Effect: A Case Study on the Qinghai–Tibetan Plateau With SMOS Data

Yu Bai, Li Jia, *Member, IEEE*, Tianjie Zhao, *Senior Member, IEEE*, Jiancheng Shi, *Fellow, IEEE*, Zhiqing Peng, Shaojie Du, Jingyao Zheng, Zhen Wang, and Dong Fan

***Abstract*—The topography can be very important for passive microwave remote sensing of soil moisture due to its complex influence on the emitted brightness temperature observed by a satellite microwave radiometer. In this study, a methodology of using the first brightness Stokes parameter (i.e., the sum of vertical and horizontal polarization brightness temperature) observed by the soil moisture and ocean salinity (SMOS) was proposed to improve the soil moisture retrieval under complex topographic conditions. The applicability of the proposed method is validated using in-situ soil moisture measurements collected at four networks (Pali, Naqu, Maqu, and Wudaoliang) on the Qinghai–Tibetan Plateau. The results over Pali, which is a typical mountainous area, showed that soil moisture retrievals using the first brightness Stokes parameter are in better agreement with the in-situ measurements (the correlation coefficient $R > 0.75$ and unbiased root mean square error <0.04 m^3/m^3) compared with that using the single-polarization brightness temperature. At the other three networks with relatively flatter terrains, soil moisture retrievals using the first brightness Stokes parameter are found to be comparable to the single-polarization retrievals. On the contrary, the maximum bias of the retrieved soil moisture caused by topographic effects exceeds 0.1 m3/m3 when using vertical or horizontal polarization alone, which is far beyond the expected accuracy (0.04 m3/m3) of SMOS satellite. In the regions on the Qinghai–Tibetan Plateau where the vegetation effect can be ignored, soil moisture retrieved using horizontal polarization brightness temperature is generally underestimated, overestimated when using vertical polarization brightness temperature. It is reasonable due to the polarization rotation effect (depolarization) caused by the topographic effects. It is concluded that the proposed method for soil moisture retrieval using the first brightness Stokes parameter has a great potential in reducing the influence of topographic effects.**

***Index Terms*—Mountain areas, Qinghai–Tibetan Plateau, soil moisture, soil moisture and ocean salinity (SMOS), the first brightness stokes parameter, topographic effects.**

Manuscript received 4 January 2023; revised 3 March 2023 and 25 March 2023; accepted 26 March 2023. Date of publication 5 April 2023; date of current version 11 May 2023. This work was supported in part by the National Natural Science Foundation of China under Grant 42090014, and in part by the Second Tibetan Plateau Scientific Expedition and Research Program under Grant 2019QZKK0103 and Grant 2019QZKK0206. *(Corresponding author: Tianjie Zhao.)*

Yu Bai, Li Jia, Tianjie Zhao, Zhiqing Peng, and Shaojie Du are with the State Key Laboratory of Remote Sensing Science, Aerospace Information Research Institute, Chinese Academy of Sciences, and University of Chinese Academy of Sciences, Beijing 100101, China (e-mail: baiyu@radi.ac.cn; jiali@aircas.ac.cn; zhaotj@aircas.ac.cn; pengzq@aircas.ac.cn; dusjmail@foxmail.com).

Jiancheng Shi is with the National Space Science Center, Chinese Academy of Sciences, Beijing 100190, China (e-mail: shijiancheng@nssc.ac.cn).

Jingyao Zheng is with the State Key Laboratory of Hydrology-Water Resources and Hydraulic Engineering, National Cooperative Innovation Center for Water Safety and Hydro-science, College of Hydrology and Water Resources, Hohai University, Nanjing 210098, China (e-mail: zhengjingyao@hhu.edu.cn).

Zhen Wang is with the National Geomatics Center of China, Beijing 100101, China (e-mail: wangzhen_2016@foxmail.com).

Dong Fan is with the Kunming University of Science and Technology, Kunming 650500, China (e-mail: dongfan@kust.edu.cn).

Digital Object Identifier 10.1109/JSTARS.2023.3264572

I. Introduction

The mountainous terrain is undulating, and the mountainous directly affect the climate and environment around it through atmospheric and hydrological processes [1], [2]. The Qinghai–Tibetan Plateau is the highest plateau in the world and also has the most complex terrain on the earth [3]. The main landcover types of the Qinghai–Tibetan Plateau include forests, grasslands, shrubs, deserts, and ice and snow, etc. The geomorphic features of the Qinghai–Tibetan Plateau include mountains, plateaus, basins and wide valleys, etc. In the Qinghai–Tibetan Plateau, not all the mountainous areas are covered by rocks. Many areas with large topographic relief are covered by meadows, shrubs or deserts in the Qinghai–Tibetan Plateau. Soil moisture plays an important role in the process of water cycle in mountainous areas of the Qinghai–Tibetan Plateau.

Many studies have shown that in the past decades, the Qinghai–Tibetan Plateau has experienced significant hydrological and climatic changes [1], [4], [5], [6], [7]. Reliable long-term soil moisture products are essential for understanding the exchanges of water and energy between the land and the atmosphere in the Qinghai–Tibetan Plateau and its impact on the climate in Eastern and Southeast Asia [1]. However, due to the complex terrain, special geographical environment and climatic conditions in the Qinghai–Tibetan Plateau (mountainous areas), it is difficult to understand the detailed process of soil moisture change due to lack of effective in-situ measurements [1], [2]. Remote sensing has become a promising method to solve these problems. Microwave remote sensing has the special capability of all-weather and all-time monitoring of soil moisture [8], [9]. Microwave L-band radiometer is considered as the optimum tool for spatial soil moisture monitoring due to its strong penetration of vegetation layer and sensitivity to surface soil moisture [10], [11], [12], [13].

At present, the soil moisture algorithms based on satellite observation mainly include the single channel algorithm (SCA) and dual-channel algorithm (DCA) [14], the multi-angular algorithm developed for SMOS [15], SMOS_IC algorithm [16], the land parameter retrieval algorithm [17], the recently developed multichannel collaborative algorithm [18] and multitemporal and multiangular approach [19], etc. The SCA algorithm uses single horizontal polarization (H_pol) or vertical polarization (V_pol) brightness temperature (TB) to retrieve soil moisture. The DCA uses H_pol and V_pol TB to simultaneously retrieve multiple parameters (such as soil moisture and vegetation optical depth). Moreover, Jackson et al. [20] and Owe et al. [17] also have tried to use H_pol and V_pol TB to retrieve multiple parameters. There is information redundancy between H_pol and V_pol TB, which makes the retrievals not robust. Konings et al. [21] found that the redundancy information from the two polarizations reduces the ability of DCA algorithm. Zhao et al. found that the degree of information (DoI) is the function of the number of observation channels (incidence angle, polarization, and frequency) [18]. Therefore, the multiangular H_pol and V_pol TB observation provided by SMOS satellite can increase the DoI for the H_pol and V_pol TBs, which provides support for simultaneous retrieval of multiple parameters (such as soil moisture and vegetation optical depth) and obtaining reliable solutions.

However, the influence of topography on the microwave emission is significant in mountainous areas [22], [23]. The microwave radiation received by the satellite radiometer may be affected by the rotation of radiation polarization plane, the shadowing effect and the multiple scattering effect between adjacent terrains and thus has a serious impact on the remote sensing of soil moisture [24].

Pierdicca et al. found that the TB bias were about 8 to 15 K at L- and X-bands due to topographic effects [25]. Luca et al. analyzed the influence of terrain slope and aspect on the microwave emission observed by satellite and found that the orientation of the linear polarization is rotated (depolarization effect) and the rotation influence on the V_pol TB is greater than that of H_pol TB [26]. Mützler et al. [27] and Kerr et al. [28] analyzed the influence of topographic effects on TB measured by spaceborne microwave radiometer, including the shadowing effect, changes of local incidence angle and the polarization rotation, which resulted in the deviation of the characteristics of the geophysical parameter to be retrieved. Talone et al. studied the changes of local incidence angle and the shadowing effects caused by the topography, and found that the change of local incidence angle caused by topography was as high as 55° when comparing incidence angle of TB values after terrain correction with that of TB under the assumed ellipsoid level of the Earth [29]. Taking the Qinghai–Tibetan Plateau as an example, Li et al. found that, due to the topographic relief, the maximum reduction of TB at V_pol was about 16 K, and the maximum increasement of TB at H_pol was 18 K, and soil moisture could be overestimated more than 0.04 m^3/m^3 due to such topographic influence [24].

Although many researchers indicated that the topographic effects have a significant impact on the microwave TB, most soil moisture retrieval algorithms assumed that the Earth's surface is horizontal, thus may fail to retrieve soil moisture over mountain areas like the Qinghai–Tibetan Plateau [30]. The current soil moisture retrieval algorithms for satellite observations normally mask out the topographic areas [31] and few studies have demonstrated the evidence of topographic effects on soil moisture retrieval at the satellite scale [24], [29]. Therefore, it is needed to quantitatively study the influence of topography on soil moisture retrievals based on spaceborne observations and explore possible solution to minimize the topography effects. Although the topographic relief may change the process of microwave radiative transfer and affects the retrieval accuracy of land surface parameters, these effects can be minimized when using the first brightness Stokes parameter (H_pol + V_pol TB) to retrieve land surface parameter (such as soil moisture). The first Stokes parameter is widely used in ocean salinity retrieval [25], [26], [32], [33], but they are rarely used in land surface soil moisture retrieval. In this study, a novel methodology that uses the sum of H_pol and V_pol TB (the first brightness Stokes parameter) was proposed to retrieve soil moisture based on the multitemporal and multiangular (MTMA) method developed in our previous study [19], which is expected to explore a solution to reduce the uncertainty of soil moisture retrievals caused by topographic effects.

This study is composed of the following parts: the data used in this study are presented in Section II; the methodologies including three retrieval strategies (single H_pol, single V_pol) and the first brightness Stokes parameter (H_pol + V_pol TB) are described in Section III; the retrieval results were presented and analyzed in Section IV; and the discussion and conclusions are given in Sections V and VI.

II. Data and Preprocessing

A. SMOS L1C Brightness Temperature

The SMOS L1C TB data are provided in icosahedral Snyder equal area earth fixed grid (ISEA-4H9), which is referred to the discrete global grid (DGG) with nodes 15 km apart [15]. The surface is in thermal equilibrium at dawn (6 A.M., usually before the sunrise) that the temperature of vegetation is expected to be close to the temperature of soil. In this study, it is assumed that vegetation canopy temperature and soil temperature are in equilibrium and expressed by the effective soil temperature, which can reduce the number of unknown variables in the algorithm. Therefore, the SMOS L1C TB data (smos-diss.eo.esa.int) at 6 A.M. (ascending orbits) are used. The two-step regression method proposed by Zhao et al. [34] was used to preprocess the SMOS L1C data so reduce the uncertainties of observed TB due to radio frequency interference (RFI) and aliasing issues [34]. The two-step regression method does not filter the SMOS L1C TB data by setting the threshold, but makes the SMOS L1C TB data closer to the theoretical expectation by refining the SMOS L1C TB data, which means that the TB data affected by RFI may also be used for the retrieval after refinement. The details of the two-step regression method are expounded in [34].

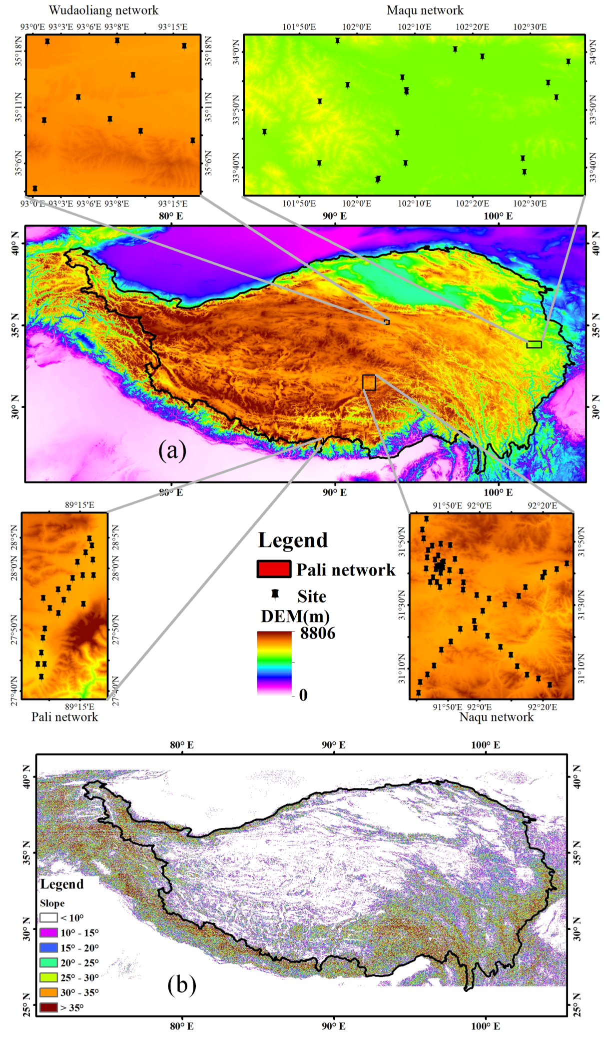

Fig. 1. Topographic distribution of the Qinghai–Tibetan Plateau. (a) Elevation. (b) Slope. The four in-situ soil moisture observation networks are given in submaps.

B. SMOS Level 3 and SMOS_IC Soil Moisture Products

The SMOS Level 3 (SMOS_L3) [15], [31], [35] and SMOS_IC version 2 (V2) (referred to as SMOS_IC) [16], [36] soil moisture products are used for comparative analysis with the retrieval results of this study. In this study, both products at 6 A.M. in 2015–2016 and 2019–2020 are downloaded from http://www.catds.fr/ and https://ib.remote-sensing.inrae.fr/.

C. Topographic Data

The shuttle radar topography mission (SRTM) data (spatial resolution of 90 m), which were jointly measured by the National Aeronautics and Space Administration and the National Imagery and Mapping Agency, were utilized to calculate the slope on the Qinghai–Tibetan Plateau [see Fig. 1(b)].

D. MODIS NDVI Product

Normalized difference vegetation index (NDVI) products (MOD13A2) in 2015–2016 from the moderate-resolution imaging spectroradiometer (MODIS) (see Fig. 2) are used as a reference to evaluate the vegetation richness on the Qinghai–Tibetan Plateau.

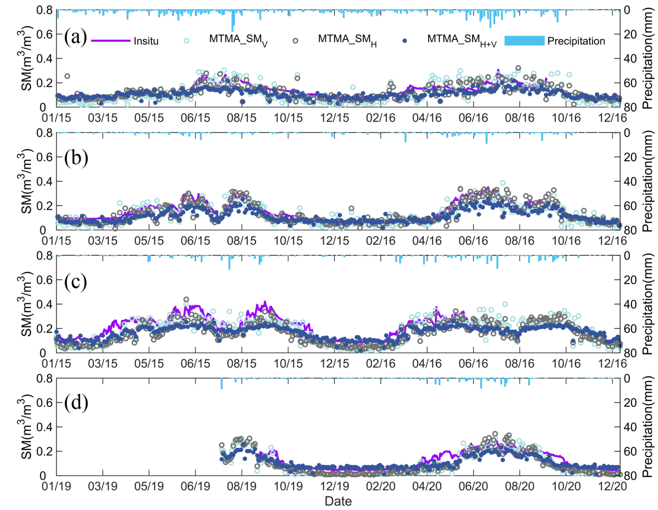

Fig. 2. Time series of soil moisture from $MTMA\_SM_{H+V}$, $MTMA\_SM_H$, and $MTMA\_SM_V$ in 2015–2016 and 2019–2020 at validation networks on the Qinghai–Tibetan Plateau. (a) Pali. (b) Maqu. (c) Naqu. (d) Wudaoliang.

TABLE I
INFORMATION OF DATASETS USED IN THIS STUDY

Variable name	Product name	Spatial resolution	Time resolution	Unit
Brightness temperature	SMOS L1C	15 km	Daily	K
Soil moisture	SMOS L3	25 km	Daily	m^3/m^3
	SMOS_IC	25 km	Daily	m^3/m^3
NDVI (MOD13C1)	MODIS	0.05°	16 days	--
The backscatter data	Sentinel-1A	10 m	12 to 24 days	dB
Elevation	SRTM	90 m	--	m
The soil temperature and precipitation	ECMWF	15 km	Daily	Soil temperature (K) Precipitation (mm)

E. European Centre for Medium-Range Weather Forecasts (ECMWF) Data

The ECMWF Reanalysis v5 (ERA5) data are a reanalysis dataset, which combines model data with observations across the world into a globally complete and consistent dataset. The data used in this study include soil layer temperature (0–7 cm) and cumulative precipitation (unit: m; precision: 0.1 mm). The spatial resolution of ECMWF ERA5 data is resampled to match the nodes spacing size (15 km) of SMOS L1C DGG TB data.

F. Sentinel-1A Backscatter Data

The C-band (5.405 GHz) radar data (descending, 6 A.M.) of Sentinel-1A, including the dual-polarization (VV + VH) backscatter data, are used to calculate the radar vegetation index (RVI = (4 ∗ VH)/(VV + VH)) [37]. The temporal resolution and spatial resolution of the Sentinel-1A data at 6 A.M. are 12 to 24 days (maximum) and 10 m, respectively. The radar data of Sentinel-1 are preprocessed for radiometric calibration, thermal noise removal and terrain correction, and resampled to 25-km spatial resolution to match the spatial resolution of SMOS soil

TABLE II
INFORMATION OF IN-SITU SOIL MOISTURE OBSERVATION NETWORKS USED FOR VALIDATION IN THIS STUDY

Network	Pali	Maqu	Naqu	Wudaoliang
Longitude range (°)	89.14-89.28	101.72-102.60	91.68-92.46	93.00- 93.29
Latitude range (°)	27.70-28.08	33.62- 34.02	31.03-31.95	35.05- 35.32
Land Cover	sparse grasslands and bare area	grasslands	grasslands	grasslands and bare area
Number of sites	21	20	57	10
Measuring depth	0-5cm	0-5cm	0-5cm	0-5cm
Slope range	0°-71.85°	0°-30.11°	0°-39.89°	0°-24.62°
Elevation standard deviation within the network	375.54 m	115.96 m	187.34 m	105.05 m

moisture products. Table I summarizes the remote sensing data used in this study.

G. In-situ Soil Moisture Network

The in-situ soil moisture data from four networks (Pali [38], Naqu [38], [39], Maqu [39], [40] and Wudaoliang) located on the Qinghai–Tibetan Plateau in China were used as validation data. The location of each validation network and the distribution of sites in each network are shown in Fig. 1(a). The Wudaoliang soil moisture and temperature monitoring network were built in 2019 with 10 sites. The range of slope and standard deviation of elevation in the area covered by each network are calculated using SRTM data with spatial resolution of 90 m to reflect the topography (see Table II). Compared with Maqu, Naqu, and Wudaoliang networks, Pali network has a wider slope range and a larger standard deviation of elevation, which means that the terrain at Pali network are more complex than the other three networks.

III. METHODOLOGY

One of the major topographic effects is the polarization rotation (depolarization) effect, which can reduce the TB values at V_pol and increase the TB values at H_pol, leading to the uncertainties of soil moisture retrieval. One possible approach for reducing topographic effects (especially the polarization rotation effect) is to apply the first brightness Stokes parameter (i.e., H_pol TB + V_pol TB) in the soil moisture retrieval algorithm. This is because the first brightness Stokes parameter remains unchanged after the polarization rotation caused by the topographic effects. The implementation of our method is composed by: 1) the SMOS L1C multi-angular TB is refined using the two-step regression method [34]; 2) the first brightness Stokes parameter is substituted into the MTMA method to replace the TB of single polarization channel [19], and then the vegetation optical depth, effective scattering albedo, soil roughness, and soil moisture are retrieved. The details of the method is described in the following sections.

A. Conception of Minimizing Topographic Effects

When the microwave radiation (TB) is affected by the topography, the polarization seen at the satellite-Earth (global reference frame) surface would be rotated with respect to that referenced to the local surface frame. The transformation from the local to the global reference frame can be expressed by the following:

$$\begin{pmatrix} \mathrm{TB}_H(\theta) \\ \mathrm{TB}_V(\theta) \end{pmatrix} = \begin{pmatrix} \cos^2(\varphi) & \sin^2(\varphi) \\ \sin^2(\varphi) & \cos^2(\varphi) \end{pmatrix} \cdot \begin{pmatrix} \mathrm{TB}_h(\theta_l) \\ \mathrm{TB}_v(\theta_l) \end{pmatrix} \tag{1}$$

where φ represents the polarization rotation angle; TB_H and TB_V are the H_pol and V_pol brightness temperature at the global reference frame with global incidence angle of θ; and TB_h and TB_v are brightness temperature at the local reference frame with local incidence angle of θ_l. The polarization rotation angle φ can be calculated by the following:

$$\sin\varphi = \sin(\beta - \beta_l) \cdot \sin(\alpha_l)/\sin(\theta_l) \tag{2}$$

where α_l, β_l are the slope angle and the azimuth angle at the local reference frame, and β is the azimuth angle at the satellite reference frame.

Equation (1) can be rewritten as follows:

$$\mathrm{TB}_H(\theta) = \mathrm{TB}_h(\theta_l) \cdot \cos^2(\varphi) + \mathrm{TB}_v(\theta_l) \cdot \sin^2(\varphi) \tag{3}$$

$$\mathrm{TB}_V(\theta) = \mathrm{TB}_h(\theta_l) \cdot \sin^2(\varphi) + \mathrm{TB}_v(\theta_l) \cdot \cos^2(\varphi) \tag{4}$$

$$\mathrm{TB}_H(\theta) + \mathrm{TB}_V(\theta) = \mathrm{TB}_h(\theta_l) + \mathrm{TB}_v(\theta_l). \tag{5}$$

Therefore, before and after the polarization rotation caused by the topographic effect, the sum of the V_pol and H_pol TB, which is referred as the first brightness Stokes parameter, is unchanged. On the other hand, many researchers have indicated that the topographic effects have the depolarization effect that increases the H_pol TB and decreases the V_pol TB [24], [27], [28], [29], and thus may bring bias to the retrieval of soil moisture [10], [24], [41] when using existing retrieval algorithms usually without considering topographic effects. In this study, we propose to use the first brightness Stokes parameter ($\mathrm{TB}_H + \mathrm{TB}_V = \mathrm{TB}_{H+V}$) to reduce topographic effects during the soil moisture retrieval.

B. Soil Moisture Retrieval Algorithm

The soil moisture retrieval algorithm used in this study is the MTMA method [19]. The MTMA method combines microwave vegetation index (MVIs) [8], [42], [43] and multitemporal method [44], [45] to decouple soil and vegetation contributions, and uses SMOS multiangular observation TB data to systematically retrieve vegetation optical depth, effective scattering albedo, surface roughness, and soil moisture.

In this study, we further introduce the first brightness Stokes parameter into to the MTMA method to minimize the topographic effects. The retrieval process of vegetation parameters

TABLE III
PARAMETERS γ_p AND μ_p FOR DIFFERENT PAIRS OF INCIDENCE ANGLES AT H_POLARIZATION AND V_POLARIZATION

	H_polarization			V_polarization		
θ_1, θ_2	γ_H	μ_H	R	γ_V	μ_V	R
15°, 30°	-0.0405	1.0146	0.9986	0.0660	0.9501	0.9986
20°, 35°	-0.0517	1.0176	0.9984	0.0842	0.9363	0.9977
25°, 40°	-0.0637	1.0190	0.9977	0.1046	0.9207	0.9962

is then given by the following:

$$\begin{cases} \mathrm{TB}_{H+V}(\theta_2) = \mathrm{TB}_H(\theta_2) + \mathrm{TB}_V(\theta_2) \\ \quad = (m_H(\theta_1,\theta_2) + m_V(\theta_1,\theta_2)) \\ + (n_H(\theta_1,\theta_2)\cdot \mathrm{TB}_H(\theta_1) + n_V(\theta_1,\theta_2) \\ \quad \cdot \mathrm{TB}_V(\theta_1)) & (6) \\ m_p(\theta_1,\theta_2) = \alpha_p(\theta_1,\theta_2)\cdot V_p^a(\theta_2) + V_p^e(\theta_2) \\ \quad - n_p(\theta_1,\theta_2) & (7) \\ n_p(\theta_1,\theta_2) = \beta_p(\theta_1,\theta_2)\cdot \frac{V_p^a(\theta_2)}{V_p^a(\theta_1)} & (8) \\ V_p^e(\theta) = (1-\Gamma_p(\theta))\cdot(1-\omega_p) \\ \quad \cdot (1+\Gamma_p(\theta))\cdot T^c & (9) \\ V_p^a(\theta) = \Gamma_p(\theta)\cdot T^s - (1-\Gamma_p(\theta)) \\ \quad \cdot (1-\omega_p)\cdot \Gamma_p(\theta)\cdot T^c & (10) \\ \min_{X = VOD_p,\ \omega_p^{\mathrm{eff}}} \mathrm{COST}_p^c(X) \\ \quad = \frac{\sum_{t=1}^{N}\sum_{i=1}^{K}\left[\mathrm{TB}_p^t(\theta_i) - \mathrm{TB}_p^{o\,t}(\theta_i)\right]^2}{\sigma(\mathrm{TB}_p^o)^2} & (11) \end{cases}$$

and the retrieval process of soil parameters are described by the following:

$$\begin{cases} E_{H+V}^s(\theta) = E_H^s(\theta) + E_V^s(\theta) \\ = (1-r_H^s(\theta))\cdot H_H + (1-r_V^s(\theta))\cdot H_V & (12) \\ H_p = A_p\cdot \exp\left(B_p\cdot Z_p^{s\,2} + C_p\cdot Z_p^s\right) & (13) \\ A_p,\ B_p,\ C_p = a_p\cdot\theta^2 + b_p\cdot\theta + c_p & (14) \\ \min_{X = SM_p,\ Z_p^s} \mathrm{COST}_p^{\mathrm{soil}}(X) \\ = \sum_{t=1}^{N}\sum_{i=1}^{K}\left[E_p^t(\theta_i) - E_p^{ot}(\theta_i)\right]^2 & (15) \end{cases}$$

where m_p and n_p are the SMOS multiangle microwave vegetation index; V_p^e and V_p^a are the vegetation emission term and attenuation term, respectively; Γ_p is the vegetation transmissivity ($\Gamma_p = \exp(--\tau_p^c/\cos(\theta))$) and is the function of $\mathrm{VOD_p}$ (τ_p^c); ω_p^{eff} is the effective scattering albedo; T^c (K) and T^s (K) are the canopy and soil temperature respectively and are assumed to be equivalent and represented by the effective soil temperature (T^{eff}), which could be gained from ancillary soil temperature data (0–7 cm) in the reanalysis data of ECMWF ERA5; γ_p and μ_p are regression constants using simulation data from the advanced integral equation model (AIEM) and their values of the two polarizations for different pairs of incidence angles are shown in the Table III; θ_1 and θ_2 are two incidence angles, for example, θ_1 is 30° and θ_2 is 40°; t is the SMOS satellite overpass time (6 A.M.); $\sigma(TB_p^o)$ (K) is the standard deviation of SMOS observed brightness temperature; TB_p (K) is simulated brightness temperature; TB_p^o (K) is SMOS observed brightness temperature; N is the number of satellite overpasses; K is the number of angles of SMOS observations; A_p, B_p, and C_p are functions of θ and obtained by regression analysis using simulation data set from AIEM [46]; E_p^s is the simulated soil emissivity; E_p^o is soil emissivity calculated using observed brightness temperature of SMOS with retrieved VOD_p and ω_p^{eff}; and X ($VOD_p, \omega_p^{\mathrm{eff}}, SM_p$, and Z_p^s) are the retrieved parameters.

It should be noted that (6) and (12) are derived by introducing the first brightness Stokes parameter into the MVIs developed by Cui et al. [42] and the bare soil emissivity model developed by Zhao et al. [46], respectively.

In this study, we find that the performance of soil moisture retrievals is satisfactory by using TB at three angle pairs ((15°, 30°), (20°, 35°), and (25°, 40°)) with an interval of 15°.

Konings et al. [21] and Zhao et al. [18] have found that the degree of information (DoI) for the H_pol and V_pol brightness temperatures is less than 2 (1< DoI <2), therefore the multitemporal TB data observed by SMOS at the 3(angle pairs)•2(polarization) = 6 channels, i.e., the dual-polarization brightness temperatures observed at three angle pairs ((15°, 30°), (20°, 35°), and (25°, 40°)) from two temporal adjacent overpasses, are used for the retrieval process in this study. Zhao et al. found that the degree of information (DoI = 1.3322∗*M*+0.4142, *M* represents the number of observation angle pairs) is the function of the number of observation angle pairs of dual-polarized TB and increases with the increase of observation angle pairs [18]. The degree of information of dual-polarized TB from six channels is 8.4. For the parameter retrieval, there are totally four parameters to be retrieved including vegetation parameters (vegetation optical depth and effective scattering albedo) and soil parameters (soil moisture and soil surface roughness). Therefore, the degree of information is sufficient to retrieve the unknown four parameters. The retrieval is performed by minimizing the cost function with the least square method.

IV. RESULTS

A. Comparison With In-Situ Measurements

To validate effectiveness of topographic effects by using the first brightness Stokes parameter for the retrievals of soil moisture, we compared the MTMA_$\mathrm{SM_{H+V}}$ retrieved by applying the first brightness Stoke parameter in the MTMA algorithm with in-situ measurements at Pali, Naqu and Maqu, and Wudaoliang soil moisture network. In addition, soil moisture retrieved using single-polarization TB (MTMA_$\mathrm{SM_H}$ for H_pol and MTMA_$\mathrm{SM_V}$ for V_pol) were also obtained. The topographic effect at the Pali network (with elevation standard deviation: 375.54 m; slope range: 0°–71.85°) is more significant than those of the other three networks (elevation standard deviation: 105.05–187.34 m; slope range: 0°–39.89°).

It should be noted that this study assumes that the MTMA method will deliver a "very dry bare soil" (low dielectric constants) output when the soil temperature is lower than 273.13 K. The soils are considered as frozen soils when the soil temperature is less than 273.15 K. Although volume scattering may exist

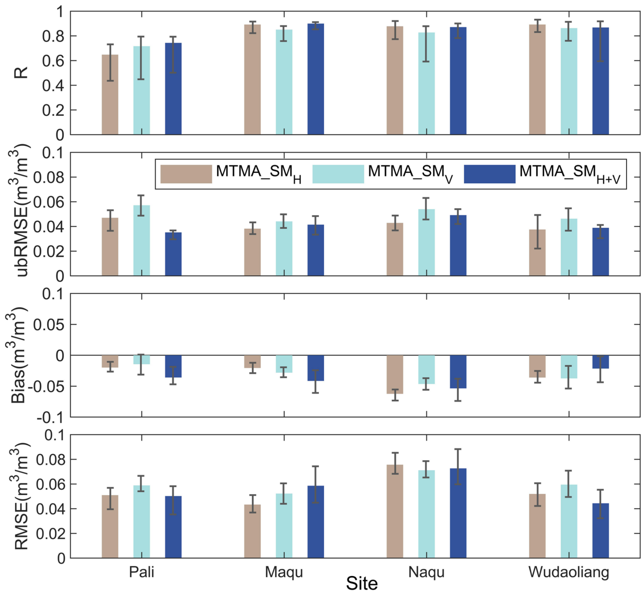

Fig. 3. Performance metrics with 95% confidence intervals for soil moisture retrievals at validation sites.

TABLE IV
QUANTITATIVE VALIDATION RESULTS OF $\text{MTMA\_SM}_{\text{H+V}}$, $\text{MTMA\_SM}_{\text{H}}$, AND $\text{MTMA\_SM}_{\text{V}}$ PRODUCTS USING IN-SITU MEASUREMENTS

		R	Bias (m^3/m^3)	RMSE (m^3/m^3)	ubRMSE (m^3/m^3)	DISO
Pali	$\text{MTMA\_SM}_{\text{H+V}}$	0.743	-0.036	0.050	0.035	0.666
	$\text{MTMA\_SM}_{\text{H}}$	0.648	-0.020	0.051	0.047	0.897
	$\text{MTMA\_SM}_{\text{V}}$	0.716	-0.014	0.059	0.057	1.040
Naqu	$\text{MTMA\_SM}_{\text{H+V}}$	0.899	-0.041	0.059	0.041	0.937
	$\text{MTMA\_SM}_{\text{H}}$	0.892	-0.021	0.043	0.038	0.870
	$\text{MTMA\_SM}_{\text{V}}$	0.850	-0.028	0.052	0.044	1.011
Maqu	$\text{MTMA\_SM}_{\text{H+V}}$	0.871	-0.054	0.073	0.049	0.917
	$\text{MTMA\_SM}_{\text{H}}$	0.877	-0.062	0.076	0.043	0.806
	$\text{MTMA\_SM}_{\text{V}}$	0.827	-0.046	0.071	0.054	1.015
Wudaoliang	$\text{MTMA\_SM}_{\text{H+V}}$	0.868	-0.022	0.044	0.039	0.858
	$\text{MTMA\_SM}_{\text{H}}$	0.892	-0.036	0.052	0.038	0.833
	$\text{MTMA\_SM}_{\text{V}}$	0.862	-0.037	0.060	0.046	1.009

with increasing penetration depth for frozen soils [47], [48], we assumed that it has only surface scattering as a very dry soil (low dielectric constants). Therefore, the liquid (unfrozen) soil moisture can be retrieved by using the Mironov's model (as used in this study) or other similar dielectric model suitable for frozen soils [49], [50].

As shown in Figs. 2 and 3, all soil moisture retrievals of $\text{MTMA\_SM}_{\text{H}}$, $\text{MTMA\_SM}_{\text{V}}$, and $\text{MTMA\_SM}_{\text{H+V}}$ at four in-situ observation networks are in good agreement with the in-situ data. The R (correlation coefficient) of MTMA_SM_{H+V} ($R = 0.743$) is slightly higher than that of $\text{MTMA\_SM}_{\text{H}}$($R = 0.648$) and $\text{MTMA\_SM}_{\text{V}}$ ($R = 0.716$), and ubRMSE (unbiased root mean square error) of $\text{MTMA\_SM}_{\text{H+V}}$ (ubRMSE $=$ 0.035 m^3/m^3) is significantly lower than that of $\text{MTMA\_SM}_{\text{H}}$ (ubRMSE $=$ 0.047 m^3/m^3) and $\text{MTMA\_SM}_{\text{V}}$ (ubRMSE $=$ 0.057 m^3/m^3) at the Pali network where the topographic effects are stronger. At Naqu, Maqu, and Wudaoliang networks with relatively flatter terrain, there is no significant difference between $\text{MTMA\_SM}_{\text{H+V}}$ and $\text{MTMA\_SM}_{\text{H}}$ and $\text{MTMA\_SM}_{\text{V}}$, no matter R or ubRMSE.

We further applied a normalized method, namely the CCHZ_distance between indices of simulation and observation (DISO) proposed by Hu et al. [51], [52] and Zhou et al. [53], to quantify the degree of improvement. This method is used to comprehensively evaluate the performance of algorithms by calculating the Euclidean distance between normalized metrics. The lower the DISO value, the better the performance of retrievals. The two metrics of R and ubRMSE are input into the CCHZ_DISO method to calculate the DISO values of $\text{MTMA\_SM}_{\text{H+V}}$, $\text{MTMA\_SM}_{\text{V}}$, and $\text{MTMA_SM}_{\text{H}}$products. It is found that at Pali network with obvious topographic effect, the DISO value of $\text{MTMA\_SM}_{\text{H+V}}$ is significantly lower than that of $\text{MTMA\_SM}_{\text{H}}$ and $\text{MTMA\_SM}_{\text{V}}$ (see Table IV). However, at the networks of Naqu, Maqu, and Wudaoliang with relatively flat terrain, the DISO values of $\text{MTMA\_SM}_{\text{H+V}}$ are lower than that of $\text{MTMA\_SM}_{\text{V}}$, and close to the DISO values of $\text{MTMA\_SM}_{\text{H}}$. It can be concluded that the topographic effect can be effectively reduced by applying the first brightness Stoke parameter in the MTMA algorithm especially for areas with stronger topographic effect.

The topographic effect can cause the rotation of the radiation polarization plane, which will lead to the depolarization of the observed TB, and then affect the soil moisture retrieval results [24], [54], such as the case at the Pali. The existing soil moisture retrieval algorithms from spaceborne radiometer observations usually without considering topographic effects and minimize the cost function between simulated and observed TB at each polarization, leading to potential errors over complex terrains. However, this polarization rotation effects may be avoided if the first brightness Stokes parameter is used to retrieve the soil moisture as done in our work.

B. Spatial Distribution Over the Qinghai–Tibetan Plateau

In this study, the $\text{MTMA\_SM}_{\text{H+V}}$, $\text{MTMA\_SM}_{\text{H}}$, and $\text{MTMA\_SM}_{\text{V}}$ were obtained over the Qinghai–Tibetan Plateau in 2015–2016 with averages as shown in Fig. 4. It was noted that the spatial distribution of the three soil moisture retrievals was generally consistent and the soil moisture in the southeast was higher than that in the northwest. Moreover, the spatial distribution of soil moisture of the three products also reflected the reasonable spatial variations of soil moisture in different climatic regions of Qinghai–Tibetan Plateau.

In this study, the number of effective retrievals (0.01 $m^3/m^3 \leq$ retrieval $\leq$ field capacity (m^3/m^3)) of each pixel on the Qinghai–Tibetan Plateau in 2015–2016 was counted as shown in Fig. 5. The numbers of effective soil moisture retrievals of the three products are relatively small in the marginal areas of the Qinghai–Tibetan Plateau, and the numbers of retrievals are relatively large in the central area of the Qinghai–Tibetan Plateau. It is worth noting that the effective retrievals of $\text{MTMA\_SM}_{\text{V}}$ (about $4.31*10^6$) and $\text{MTMA\_SM}_{\text{H}}$ (about $6.19*10^6$) are fewer than that of $\text{MTMA\_SM}_{\text{H+V}}$ (about $7.12*10^6$). The main reason

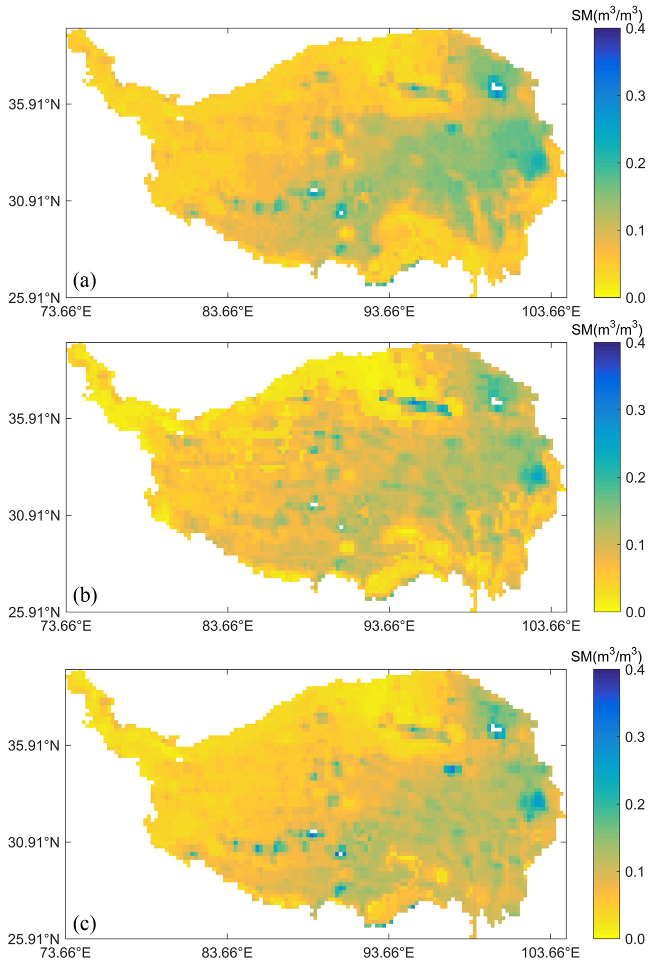

Fig. 4. Spatial distribution of the time-averaged soil moisture in 2015-2016 on the Qinghai–Tibetan Plateau: (a) MTMA_$\mathrm{SM_V}$. (b) MTMA_$\mathrm{SM_{H+V}}$. (c) MTMA_$\mathrm{SM_H}$.

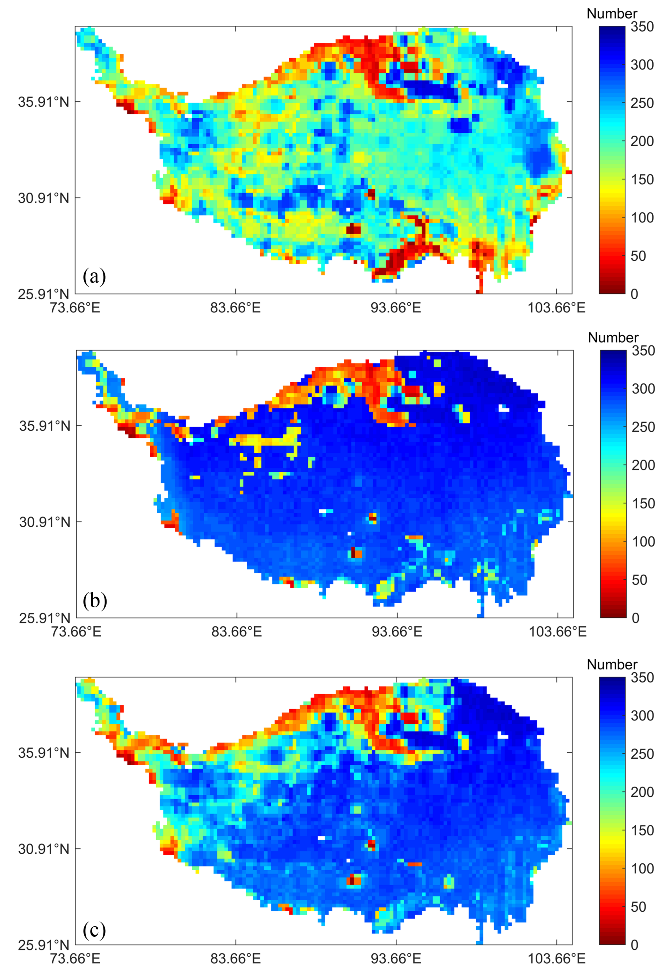

Fig. 5. Spatial distribution of the effective number of soil moisture retrievals in each pixel on the Qinghai–Tibetan Plateau in 2015–2016. (a) MTMA_$\mathrm{SM_V}$. (b) MTMA_$\mathrm{SM_{H+V}}$. (c) MTMA_$\mathrm{SM_H}$.

may be that the topographic effect led to the decreasing of V_pol TB and the increasing H_pol TB, leading to the soil moisture retrieval beyond its physical range.

The topography can change the radiation process of ground TB and cause the change of surface emissivity, and finally lead to the retrieval bias of soil moisture using conventional retrieval algorithm. To evaluate the influence of topographic effect on soil moisture retrievals, soil moisture difference ($\Delta\mathrm{SM_p} = (\mathrm{MTMA\_SM_p}) - (\mathrm{MTMA\_SM_{H+V}})$) between soil moisture retrieved without and with the consideration of topographic effect is calculated as show in Fig. 6. According to the product of 16-day MODIS NDVI and RVI, only regions from Qinghai–Tibetan Plateau with NDVI less than 0.4 and RVI less than 0.3 were extracted respectively, where the vegetation effect on soil moisture retrievals is minimal. The aim is to compare the impact of differences in vegetation information derived from optical and microwave remote sensing data on the subsequent analysis. Although the regions extracted based on NDVI threshold or RVI threshold contains the regions with less than 10° slope range, the regions are less affected by vegetation and could be used to explore the topography effects.

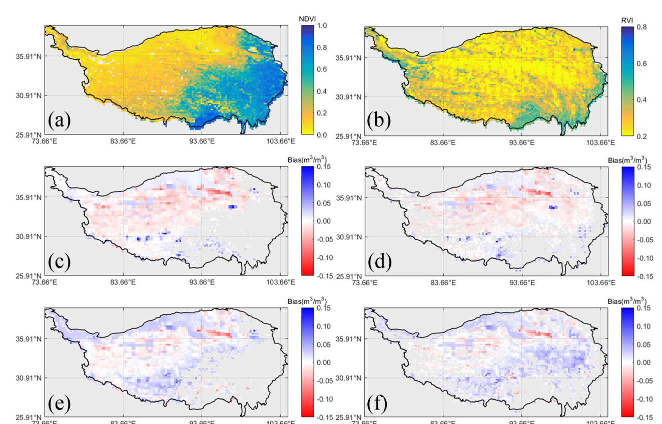

Fig. 6. Spatial distribution of vegetation index and soil moisture difference ($\Delta\mathrm{SM_p}$) on the Qinghai–Tibetan Plateau in 2015–2016. (a) NDVI. (b) RVI. (c) $\Delta\mathrm{SM_H}$ for H_pol (($\mathrm{MTMA\_SM_H}$)$-$($\mathrm{MTMA\_SM_{H+V}}$)) within NDVI less than 0.4. (d) $\Delta\mathrm{SM_H}$ for H_pol (($\mathrm{MTMA\_SM_H}$)$-$($\mathrm{MTMA\_SM_{H+V}}$)) within RVI less than 0.3. (e) $\Delta\mathrm{SM_V}$ for V_pol (($\mathrm{MTMA\_SM_V}$)$-$($\mathrm{MTMA\_SM_{H+V}}$)) within NDVI less than 0.4. (f) $\Delta\mathrm{SM_V}$ for V_pol (($\mathrm{MTMA\_SM_V}$)$-$($\mathrm{MTMA\_SM_{H+V}}$)) within RVI less than 0.3.

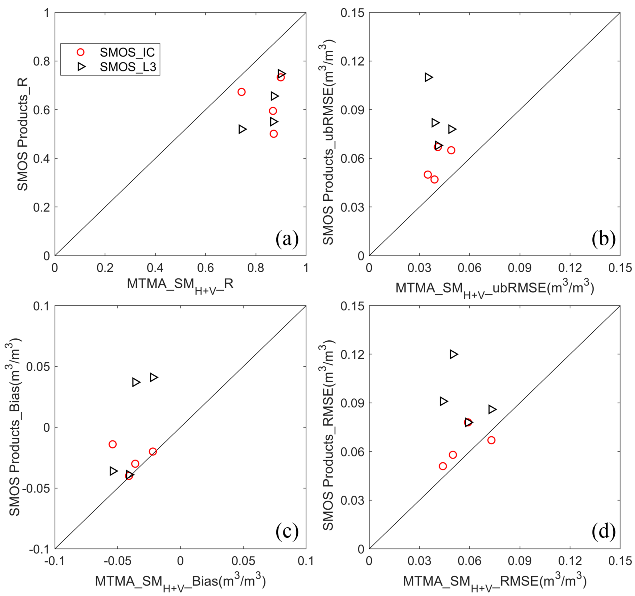

Fig. 7. Metrics of MTMA_SM$_{\mathrm{H+V}}$ versus the metrics of SMOS_IC and SMOS_L3 products at 4 validation networks on the Qinghai–Tibetan Plateau in 2015–2016 and 2019–2020.

TABLE V
QUANTITATIVE VALIDATION RESULTS OF MTMA_SM$_{\mathrm{H+V}}$, SMOS_L3, AND SMOS_IC PRODUCTS USING IN-SITU MEASUREMENTS

		R	Bias (m^3/m^3)	RMSE (m^3/m^3)	ubRMSE (m^3/m^3)
Pali	MTMA_SM$_{\mathrm{H+V}}$	0.743	-0.036	0.050	0.035
	SMOS_IC	0.673	-0.030	0.058	0.050
	SMOS_L3	0.520	0.037	0.120	0.110
Naqu	MTMA_SM$_{\mathrm{H+V}}$	0.899	-0.041	0.059	0.041
	SMOS_IC	0.733	-0.040	0.078	0.067
	SMOS_L3	0.748	-0.039	0.078	0.068
Maqu	MTMA_SM$_{\mathrm{H+V}}$	0.871	-0.054	0.073	0.049
	SMOS_IC	0.501	-0.014	0.067	0.065
	SMOS_L3	0.656	-0.036	0.086	0.078
Wudaoliang	MTMA_SM$_{\mathrm{H+V}}$	0.868	-0.022	0.044	0.039
	SMOS_IC	0.595	-0.020	0.051	0.047
	SMOS_L3	0.551	0.041	0.091	0.082

It is found that $\Delta\mathrm{SM_H}$ was generally smaller than 0 and $\Delta\mathrm{SM_V}$ was generally greater than 0 in most areas although the slope in some areas was less than 10°, indicating that soil moisture retrieved based on single H_pol TB was underestimated, while soil moisture retrieved by the single V_pol TB was overestimated. Similarly, Li et al. [24] have found that the topographic effect led to the decreasing of V_pol TB and the increasing of H_pol TB in most areas of the Qinghai–Tibetan Plateau (including areas with the slope <10°), which leads to overestimation or underestimation of soil moisture.

According to the statistical results, the maximum bias of soil moisture of MTMA_SM$_{\mathrm{H}}$ and MTMA_SM$_{\mathrm{V}}$ even exceeds 0.1 m^3/m^3 in some areas with large terrain fluctuation (the elevation difference exceeding 1000 m and the slope exceeding 35°), which is far beyond the expected accuracy (0.04 m^3/m^3) of SMOS satellite.

V. DISCUSSIONS

A. Comparison With SMOS Products

In this study, we also compared the new soil moisture retrievals considering topographic effects with the values from SMOS_L3 and SMOS_IC soil moisture products. In order to match the spatial resolution (25 km) of SMOS_L3 and SMOS_IC soil moisture products, the retrieved soil moisture with the spatial resolution of 15 km using MTMA method were resampled to 25-km spatial resolution.

According to the Fig. 7 and statistical metrics in Table V, the retrievals of MTMA_SM$_{\mathrm{H+V}}$ at four networks are in better agreement with the in-situ data than SMOS_L3 and SMOS_IC products. The overall correlation coefficient (R = 0.828) is higher than that of SMOS_IC (R = 0.626) and SMOS_L3 (R = 0.619) products. The overall ubRMSE (0.041 m^3/m^3) of the MTMA_SM$_{\mathrm{H+V}}$ at all validation networks is also lower than that of SMOS_IC (ubRMSE = 0.057 m^3/m^3) and SMOS_L3 (ubRMSE = 0.085 m^3/m^3) products, which is closer to the expected accuracy of the SMOS mission. Therefore, the quantitative validation results of MTMA_SM$_{\mathrm{H+V}}$ confirmed that the performance of soil moisture retrievals of the method proposed in this study are significantly better than current SMOS_L3 and SMOS_IC soil moisture products, indicating the advantage of the proposed method to reduce the topographic effects where terrain relief is strong, like in the Qinghai–Tibetan Plateau.

B. Impact of the Vegetation Effects

When the depth of vegetation layer increases, the signal from the soil layer may not be observed by the microwave sensor onboard satellites due to low penetration through the vegetation layer. Moreover, dense vegetation might significantly weaken the angle-dependent variability of the observed TB and lead to less degree of information to be used to retrieve the effective vegetation optical depth. The MTMA method used in this study is sensitive to the variability of TB with incidence angles. Therefore, in dense vegetation areas, the uncertainty of retrieved vegetation optical depth is relatively larger, since the difference in TB between different observation angles was small because of significant vegetation effects [32].

For most areas with dense vegetation cover over large terrain relief on the Qinghai–Tibetan Plateau, the microwave radiation was affected by both topography effects and vegetation effects (not shown in this study). Li et al. [24] found that the bias of TB (H_pol or V_pol) caused by topographic effects (slope and aspect) is about 10–15 K through simulation experiments. Talone et al. found that the error in TB caused by the vegetation layer also exceeded 10 K [29]. Vegetation has the depolarization effect similar as the topographic effect and it can be more significant than that from the topographic effect. The uncertainty of soil moisture retrieval associated with vegetation effects might lead to an obscuration of topography effects. For example, the overestimation or underestimation of vegetation effects at H_pol or V_pol may lead to overestimation or underestimation of soil moisture. Therefore, for densely vegetated areas, it could be very complex to distinguish vegetation effects and topography effects, and the dense vegetation areas are out of the scope in this study.

VI. Conclusion

Passive microwave remote sensing can provide important tool for soil moisture monitoring in mountainous areas. In this study, we proposed a methodology to apply the first brightness Stokes parameter (the sum of H_pol and V_pol TB) in the MTMA method to reduce the influence of topographic effects on soil moisture retrieval.

According to the validation results using in-situ data at the four ground networks (Pali, Naqu, Maqu, and Wudaoliang networks), it is found that soil moisture retrievals using the first brightness Stokes parameter are in better agreement with in-situ measurements (the $R > 0.75$ and ubRMSE < 0.04 m^3/m^3) compared to the single-polarization retrievals at Pali network where severely topographic effects exist. In the other three networks with flatter terrain, the performance of soil moisture retrievals using the first brightness Stokes parameter is still comparable with that using single-polarization TB observations. In addition, by analyzing the soil moisture retrievals on the Qinghai–Tibetan Plateau for the conditions with less vegetation effects (NDVI $<$ 0.4 or RVI $<$ 0.3), it was found that the soil moisture using H_pol TB is generally underestimated and that of using V_pol TB is generally overestimated, which is expected due to the depolarization effect caused by the topography. However, this method may need a further detailed review in densely vegetated areas, as the effects of vegetation may obscure the effects of topography. In general, our method applying the first brightness Stokes parameter (the sum of H_pol and V_pol TB) in the MTMA method is a simple and feasible solution to deal with the topographic effects, and the results showed a considerable improvement in mountainous areas such as the Qinghai–Tibetan Plateau.

Acknowledgment

In-situ soil moisture data are contributed by the Pali and Naqu Soil Moisture Network supported by the Ministry of Education Key Laboratory for Earth System Modeling, and Center for Earth System Science, Tsinghua University.

References

[1] J. Zeng et al., "Evaluation of remotely sensed and reanalysis soil moisture products over the Tibetan Plateau using in-situ observations," *Remote Sens. Environ.*, vol. 163, pp. 91–110, 2015.

[2] Z. Su et al., "The Tibetan Plateau observatory of plateau scale soil moisture and soil temperature (Tibet-Obs) for quantifying uncertainties in coarse resolution satellite and model products," *Hydrol. Earth Syst. Sci.*, vol. 15, no. 7, pp. 2303–2316, 2011.

[3] L. Zhao et al., "Spatiotemporal analysis of soil moisture observations within a Tibetan mesoscale area and its implication to regional soil moisture measurements," *J. Hydrol.*, vol. 482, pp. 92–104, 2013.

[4] K. Yang et al., "Response of hydrological cycle to recent climate changes in the Tibetan Plateau," *Climatic Change*, vol. 109, nos. 3/4, pp. 517–534, 2011.

[5] K. Yang et al., "Recent climate changes over the Tibetan Plateau and their impacts on energy and water cycle: A review," *Glob. Planet. Change*, vol. 112, pp. 79–91, 2014.

[6] S. Kang et al., "Review of climate and cryospheric change in the Tibetan Plateau," *Environ. Res. Lett.*, vol. 5, no. 1, pp. 15101–15101, 2010.

[7] P. Zhang et al., "A dataset of 10-year regional-scale soil moisture and soil temperature measurements at multiple depths on the Tibetan Plateau," *Earth Syst. Sci. Data*, vol. 14, no. 12, pp. 5513–5542, 2022.

[8] J. Shi et al., "Airborne and spaceborne passive microwave measurements of soil moisture," *Observ. Meas. Ecohydrological Processes*, vol. 2, pp. 71–105, 2019.

[9] D. Zheng et al., "Active and passive microwave signatures of diurnal soil freeze-thaw transitions on the Tibetan Plateau," *IEEE Trans. Geosci. Remote Sens.*, vol. 60, 2022, Art. no. 4301814.

[10] Y. H. Kerr, P. Waldteufel, J. - P. Wigneron, J. Martinuzzi, J. Font, and M. Berger, "Soil moisture retrieval from space: The soil moisture and ocean salinity (SMOS) mission," *IEEE Trans. Geosci. Remote Sens.*, vol. 39, no. 8, pp. 1729–1735, Aug. 2001.

[11] D. Zheng et al., "Impact of soil permittivity and temperature profile on L-band microwave emission of frozen soil," *IEEE Trans. Geosci. Remote Sens.*, vol. 59, no. 5, pp. 4080–4093, May 2021.

[12] J. Zheng et al., "Assessment of 24 soil moisture datasets using a new in situ network in the Shandian River basin of China," *Remote Sens. Environ.*, vol. 271, 2022, Art. no. 112891.

[13] T. Zhao et al., "Soil moisture experiment in the Luan River supporting new satellite mission opportunities," *Remote Sens. Environ.*, vol. 240, 2020, Art. no. 111680.

[14] M. J. Chaubell et al., "Improved SMAP dual-channel algorithm for the retrieval of soil moisture," *IEEE Trans. Geosci. Remote Sens.*, vol. 58, no. 6, pp. 3894–3905, Jun. 2020.

[15] Y. H. Kerr et al., "The SMOS soil moisture retrieval algorithm," *IEEE Trans. Geosci. Remote Sens.*, vol. 50, no. 5, pp. 1384–1403, May 2012.

[16] R. Fernandez-Moran et al., "SMOS-IC: An alternative SMOS soil moisture and vegetation optical depth product," *Remote Sens.*, vol. 9, no. 5, 2017, Art. no. 457.

[17] M. Owe, R. de Jeu, and J. Walker, "A methodology for surface soil moisture and vegetation optical depth retrieval using the microwave polarization difference index," *IEEE Trans. Geosci. Remote Sens.*, vol. 39, no. 8, pp. 1643–1654, Aug. 2001.

[18] T. Zhao et al., "Retrievals of soil moisture and vegetation optical depth using a multi-channel collaborative algorithm," *Remote Sens. Environ.*, vol. 257, 2021, Art. no. 112321.

[19] Y. Bai et al., "A multi-temporal and multi-angular approach for systematically retrieving soil moisture and vegetation optical depth from SMOS data," *Remote Sens. Environ.*, vol. 280, 2022, Art. no. 113190.

[20] T. J. Jackson, A. Y. Hsu, and P. E. O"Neill, "Surface soil moisture retrieval and mapping using high-frequency microwave satellite observations in the southern great plains," *J. Hydrometeorol.*, vol. 3, no. 6, pp. 688–699, 2002.

[21] A. G. Konings, K. A. McColl, M. Piles, and D. Entekhabi, "How many parameters can be maximally estimated from a set of measurements?," *IEEE Geosci. Remote Sens. Lett.*, vol. 12, no. 5, pp. 1081–1085, May 2015.

[22] Y. Guo, *Study on Terrain Correction of Passive and Active Microwave Measurements and Soil Moisture Retrieval Combining Passive and Active Microwave Remote Sensing*. Beijing, China: Inst. Remote Sens. Appl. Chin. Acad. Sci., pp. 1–20, 2009.

[23] A. Mialon, L. Coret, Y. H. Kerr, F. Secherre, and J. - P. Wigneron, "Flagging the topographic impact on the SMOS signal," *IEEE Trans. Geosci. Remote Sens.*, vol. 46, no. 3, pp. 689–694, Mar. 2008.

[24] X. Li et al., "Relief effects of mountain areas on soil moisture retrieval using passive C-band: A case study in Qinghai-Tibet Plateau," *J. Remote Sens.*, vol. 16, no. 4, pp. 850–867, 2012.

[25] E. Valencia et al., "Improving the accuracy of sea surface salinity retrieval using GNSS-R data to correct the sea state effect," *Radio Sci.*, vol. 46, no. 6, pp. 1–11, 2011.

[26] H. Li et al., "Correlation of SMOS satellite sea surface brightness temperature data and the sea surface salinity data," *Remote Sens. Technol. Appl.*, vol. 31, no. 1, pp. 143–148, 2016.

[27] C. Mätzler and A. Standley, "Technical note: Relief effects for passive microwave remote sensing," *Int. J. Remote Sens.*, vol. 21, no. 12, pp. 2403–2412, 2010.

[28] Y. H. Kerr, F. Sécherre, J. Lastenet, and J.-P. Wigneron, "SMOS: Analysis of perturbing effects over land surfaces," in *Proc. IEEE Int. Geosci. Remote Sens. Symp.*, 2003, vol. 2, pp. 908–910.

[29] T. Marco, A. Camps, A. Monerris, M. Vall-llossera, P. Ferrazzoli, and M. Piles, "Surface topography and mixed-pixel effects on the simulated l-band brightness temperatures," *IEEE Trans. Geosci. Remote Sens.*, vol. 45, no. 7, pp. 1996–2003, Jul. 2007.
[30] I. E. Mladenova et al., "Remote monitoring of soil moisture using passive microwave-based techniques — Theoretical basis and overview of selected algorithms for AMSR-E," *Remote Sens. Environ.*, vol. 144, pp. 197–213, 2014.
[31] A. Al Bitar et al., "The global SMOS level 3 daily soil moisture and brightness temperature maps," *Earth Syst. Sci. Data*, vol. 9, no. 1, pp. 293–315, 2017.
[32] H. Lu, Z. Wang, and X. Yin, "Research of the sea surface salinity retrieval method based on SMOS data," *Remote Sens. Technol. Appl.*, vol. 29, no. 3, pp. 401–409, 2014.
[33] D. M. Le Vine and S. Abraham, "The effect of the ionosphere on remote sensing of sea surface salinity from space: Absorption and emission at L band," *IEEE Trans. Geosci. Remote Sens.*, vol. 40, no. 4, pp. 771–782, Apr. 2002.
[34] T. Zhao et al., "Refinement of SMOS multiangular brightness temperature toward soil moisture retrieval and its analysis over reference targets," *IEEE J. Sel. Topics Appl. Earth Observ. Remote Sens.*, vol. 8, no. 2, pp. 589–603, Feb. 2015.
[35] N. Reul et al., "Sea surface salinity observations from space with the SMOS satellite: A new means to monitor the marine branch of the water cycle," *Surv. Geophys.*, vol. 35, no. 3, pp. 681–722, 2013.
[36] J.-P. Wigneron et al., "SMOS-IC data record of soil moisture and L-VOD: Historical development, applications and perspectives," *Remote Sens. Environ.*, vol. 254, 2021, Art. no. 112238.
[37] D. Mandal et al., "Dual polarimetric radar vegetation index for crop growth monitoring using sentinel-1 SAR data," *Remote Sens. Environ.*, vol. 247, 2020, Art. no. 111954.
[38] Y. Chen et al., "Evaluation of SMAP, SMOS, and AMSR2 soil moisture retrievals against observations from two networks on the Tibetan Plateau," *J. Geophysical Res.: Atmospheres*, vol. 122, no. 11, pp. 5780–5792, 2017.
[39] P. Zhang et al., "Status of the Tibetan Plateau observatory (Tibet-Obs) and a 10-year (2009-2019) surface soil moisture dataset," *Earth Syst. Sci. Data*, vol. 13, no. 6, pp. 3075–3102, 2021.
[40] L. Dente et al., "Maqu network for validation of satellite-derived soil moisture products," *Int. J. Appl. Earth Observ. Geoinf.*, vol. 17, pp. 55–65, 2012.
[41] L. Fan et al., "Mapping soil moisture at a high resolution over mountainous regions by integrating in situ measurements, topography data, and MODIS land surface temperatures," *Remote Sens.*, vol. 11, no. 6, 2019, Art. no. 656.
[42] Q. Cui, J. Shi, J. Du, T. Zhao, and C. Xiong, "An approach for monitoring global vegetation based on multiangular observations from SMOS," *IEEE J. Sel. Topics Appl. Earth Observ. Remote Sens.*, vol. 8, no. 2, pp. 604–616, Feb. 2015.
[43] J. Shi et al., "Microwave vegetation indices for short vegetation covers from satellite passive microwave sensor AMSR-E," *Remote Sens. Environ.*, vol. 112, no. 12, pp. 4285–4300, 2008.
[44] A. G. Konings et al., "Vegetation optical depth and scattering albedo retrieval using time series of dual-polarized L-band radiometer observations," *Remote Sens. Environ.*, vol. 172, pp. 178–189, 2016.
[45] A. G. Konings et al., "L-band vegetation optical depth and effective scattering albedo estimation from SMAP," *Remote Sens. Environ.*, vol. 198, pp. 460–470, 2017.
[46] T. Zhao et al., "Parametric exponentially correlated surface emission model for L-band passive microwave soil moisture retrieval," *Phys. Chem. Earth, Parts A/B/C*, vol. 83-84, pp. 65–74, 2015.
[47] T. Zhao et al., "A new soil freeze/thaw discriminant algorithm using AMSR-E passive microwave imagery," *Hydrological Processes*, vol. 25, no. 11, pp. 1704–1716, 2011.
[48] T. Zhao et al., "Measurement and modeling of multi-frequency microwave emission of soil freezing and thawing processes," in *Proc. Prog. Electromagn. Res. Symp.*, 2018, pp. 31–36.
[49] L. Zhang, T. Zhao, L. Jiang, and S. Zhao, "Estimate of phase transition water content in freeze–thaw process using microwave radiometer," *IEEE Trans. Geosci. Remote Sens.*, vol. 48, no. 12, pp. 4248–4255, Dec. 2010.
[50] S. Wu, T. Zhao, J. Pan, H. Xue, L. Zhao, and J. Shi, "Improvement in modeling soil dielectric properties during freeze-thaw transitions," *IEEE Geosci. Remote Sens. Lett.*, vol. 19, 2022, Art. no. 2001005.
[51] Z. Hu et al., "CCHZ-DISO: A timely new assessment system for data quality or model performance from Da Dao Zhi Jian," *Geophys. Res. Lett.*, vol. 49, no. 23, 2022, Art. no. 100681.
[52] Z. Hu et al., "DISO: A rethink of Taylor diagram," *Int. J. Climatol.*, vol. 39, no. 5, pp. 2825–2832, 2019.
[53] Q. Zhou et al., "Decompositions of Taylor diagram and DISO performance criteria," *Int. J. Climatol.*, vol. 41, no. 12, pp. 5726–5732, 2021.
[54] Y. Guo et al., "Evaluation of terrain effect on microwave radiometer measurement and its correction," *Int. J. Remote Sens.*, vol. 32, no. 24, pp. 8899–8913, 2011.

Yu Bai received the B.S. degree in geographical information system from Shanxi Agricultural University, Jinzhong, China, in 2015, and the master's degree in cartography and geographical information system from Jilin University, Changchun, China, in 2018. He is currently working toward the Ph.D. degree in the Aerospace Information Research Institute, Chinese Academy of Sciences, Beijing, China.

His research interests include the research of soil moisture retrieval algorithm of passive microwave remote sensing and the validation of soil moisture products.

Li Jia (Member, IEEE) received the B.S. degree in dynamic meteorology from the Beijing College of Meteorology, Beijing, China, in 1988, the M.Sc. degree in atmospheric physics from the Chinese Academy of Sciences, Beijing, in 1997, and the Ph.D. degree in environmental science from Wageningen University, Wageningen, The Netherlands, in 2004.

She is currently a Professor with the State Key Laboratory of Remote Sensing Science, Aerospace Information Research Institute, Chinese Academy of Sciences. Her research interests include the study of earth observation and its applications in hydrometeorology, water resource, agriculture, and climate change.

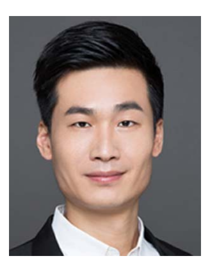

Tianjie Zhao (Senior Member, IEEE) received the B.S. and Ph.D. degrees in cartography and geographical information system from Beijing Normal University, Beijing, China, in 2007 and 2012, respectively.

From 2010 to 2012, he was a Visiting Scientist with the Hydrology and Remote Sensing Laboratory, Agricultural Research Service, U.S. Department of Agriculture, Beltsville, MD, USA. He is currently an Associate Professor with the State Key Laboratory of Remote Sensing Science, Aerospace Information Research Institute, Chinese Academy of Sciences, Beijing. His research interests include microwave remote sensing of soil moisture and its freeze-thaw process.

Dr. Zhao was the recipient of the scholarship award for excellent doctoral student granted by the Ministry of Education of China in 2011, the Young Scientist Award from the International Union of Radio Science (in 2014, and the Young Scientist Award from Progress in Electromagnetics Research Symposium in 2018.

Jiancheng Shi (Fellow, IEEE) received the B.A. degree in hydrogeology and geological engineering from the University of Lanzhou, Lanzhou, China, in 1982, and the M.A. and Ph.D. degrees in geography from the University of California, Santa Barbara (UCSB), Santa Barbara, CA, USA, in 1987 and 1991, respectively.

He was a Research Professor with the Institute for Computational Earth System Sciences, UCSB. In 2010, he became the Director and Senior Research Scientist with the State Key Laboratory of Remote Sensing Science, sponsored by the Aerospace Information Research Institute, Chinese Academy of Sciences and Beijing Normal University, Beijing, China. He was the PI of the Water Cycle Observation Mission. He is currently a Senior Research Scientist with National Space Science Center, Chinese Academy of Sciences, Beijing. His research interests include microwave remote sensing and global water cycle studies.

Zhiqing Peng is currently working toward the Ph.D. degree in the Aerospace Information Research Institute, Chinese Academy of Sciences, Beijing, China.

His research interests include microwave remote sensing of soil moisture retrieval and data fusion at L-band.

Shaojie Du received the bachelor's degree in geographic information system from Zhengzhou University, Zhengzhou, China, in 2015, and the master's degree in cartography and geographical information system from the University of Chinese Academy of Sciences, Beijing, China, in 2022.

His research interests include active microwave remote sensing. From 2019 to 2022, he studied the mechanism of microwave remote sensing and the retrieval of soil moisture with the Water Cycle Laboratory, State Key Laboratory of Remote Sensing Science.

Jingyao Zheng is currently working toward the Ph.D. degree in the College of Hydrology and Water Resources, Hohai University, Nanjing, China.

His research interests include the spatial downscaling of satellite-based soil moisture for hydrological applications.

Zhen Wang received the B.S. degree in geographical information system from Shandong University of Science and Technology, Qingdao, China, in 2014, and the Ph.D. degree from China University of Mining & Technology (Beijing), Beijing, China, in 2021.

He is currently an Engineer with the National Geomatics Center of China, Beijing. His research interests include soil moisture retrieval from active and passive microwave remote sensing.

Dong Fan received the Ph.D. degree in cartography and geographical information system from the University of Chinese Academy of Sciences, Beijing, China, in 2003.

He is currently a Lecturer with the Kunming University of Science and Technology, Kunming, China. His research interests include the microwave remote sensing of soil moisture and the spatiotemporal fusion, and the downscaling of remotely sensed products.